DOI: 10.61782/fa.2025.0810

FORUM ACUSTICUM EURONOISE 2025

# SPATIAL CHARACTERIZATION OF NOISE GENERATED BY A DRONE IN HOVERING FLIGHT

**Alberto Izquierdo**[1*] **Lara del Val**[1] **Juan J. Villacorta**[1] **Javier Retortillo**[1]
[1] Department of Signal Theory and Communications and Telematics Engineering, University of Valladolid, Spain

## ABSTRACT

The result enables the design of deterministic beamformers with low computational load or optimal LCMV beamformers that incorporate these constraints to enhance acoustic detection. To enable the detection of acoustic events during drone flights—such as screams, whistles, or gunshots—it is crucial to mitigate the noise generated by the drone's motors. The primary strategies for noise reduction include acoustic array isolation, frequency-domain filtering, and spatial filtering via beamforming. Advanced beamforming algorithms allow the creation of radiation nulls at specific locations, either predefined or adaptively determined.

This study utilizes a ground-based acoustic array composed of 810 MEMS microphones to characterize the spatial and spectral noise profile of a 4.5 kg hexacopter drone hovering at altitudes of 2 and 5 meters. The processing pipeline used to derive spatial responses is detailed, revealing that the dominant noise sources are located at the propeller tips and their intersections.

The findings support the design of deterministic beamformers with low computational complexity, as well as the development of optimal LCMV (Linearly Constrained Minimum Variance) beamformers that incorporate spatial constraints to improve the detection of relevant acoustic events.

**Keywords:** *MEMS microphone array, beamforming, drone, propeller.*

[*] ***Corresponding author**: alberto.izquierdo@uva.es*


## 1. INTRODUCTION

Surveillance and rescue systems are traditionally drone-based and incorporate a suite of sensors including optical cameras, infrared cameras, Lidar and microwave radars [1].

Acoustic sensors are now being incorporated into drones, initially by installing a small array of microphones in circular or star topologies, typically between 8 and 32 microphones [2]. The challenge is to discriminate the acoustic noise produced by the drone, called 'Ego Noise', from acoustic signals of a weak nature to be detected in a surveillance and rescue system, typically cries for help, whistles, etc.

Using MEMS microphones, it is possible to build arrays with a significant number of microphones, typically between 100 and 200, which allow beamforming techniques to be used. With these techniques, it is feasible to position radiation nulls in the directions where the drone's acoustic noise is generated, associated with its propulsion system formed by the engines and propellers [3-5].

In this way, on-board acoustic arrays can be implemented in a drone, which, knowing the spatial positions of the noise generated by the drone and using statistically optimal beamforming algorithms, significantly cancel the ego noise.

Precisely in order to characterize and precisely locate the noise generated by a drone and based on the experience of the research group, a high-resolution acoustic array has been used to spatially characterize the noise generated by a medium-sized drone consisting of 6 motors with a wingspan of 80 cm and a MTOW of 4.5 kg. Figures 1 and 2 show respectively the acoustic array and the drone under test.

## 2. ACOUSTIC SYSTEM

The developed acoustic system comprises three components:

- An array of MEMS microphones for acoustic sensing.
- An FPGA/Processor-based system for acquisition and pre-processing.
- A PC application for analysis, detection, and visualization.

**Figure 1**. Array of MEMS microphones.

**Figure 2**. Drone under flight test.

### 2.1 Array of MEMS microphones

In this research, a two-dimensional arrangement of 486 SPH0641LU4H-1 digital MEMS microphones from Knowles [6], featuring a spatial aperture of approximately 35 cm in each spatial dimension, has been employed. This 2D array is displayed in Fig. 1. For practical applications (implementation of digital band-pass filters), the frequency range of interest has been established between 12 kHz and 48 kHz. This frequency range leverages the selected MEMS microphones' high sensitivity to high frequencies while minimizing ambient noise interference by eliminating low frequencies. In conjunction with the array, the delay-and-sum beamforming method has been applied under near-field conditions [7]. Consequently, a spherical wavefront propagation model has been assumed.

### 2.2 Drone description

We have worked with a professional drone Model DT6SP manufactured by the company DronTecnic as shown in figure 3. This drone consists of 6 Tarot 4108 motors of 380kv of 300W with an individual weight of 112 gr. Each motor is equipped with 13 by 5.5” propellers that provide a maximum thrust of 1,620 grams per motor. It also incorporates a Pixhawk 2.1 autopilot along with a 3DR Datalink (433Mhz) telemetry system and FrSky remote control transmitter (100 mw/ 2.4Ghz) with a range of 2,000m. The system uses a 6-cell 8,000mA LIPO battery with a weight of 1080 gr. Its dimensions are 760mm x 685mm x 300mm, with a diameter between rotors of 685mm. The empty weight is 2.3kg and has a MTOW of 4.5kg. The drone can operate at a maximum altitude of 120m with an autonomy of 20 minutes in stationary flight. The maximum speed is 14 m/s and the typical ascent/descent speed is 2 m/s.

### 2.3 Acquisition and processing system

Five interconnected and synchronized National Instruments sbRIO-9607 platforms [8] were employed to acquire the signals captured by the array's MEMS microphones. Each sbRIO-9607 is an embedded single-board controller that integrates a Xilinx Zynq-7020 system-on-chip, featuring a dual-core ARM processor operating at 667 MHz and a programmable FPGA. In this configuration, 81 out of the 96 available digital input/output (I/O) lines of the FPGA are used in a multiplexed manner to interface with 162 MEMS microphones. Consequently, a total of five sbRIO units are required to accommodate the full array of 810 microphones. The remaining FPGA I/O lines are dedicated to generating the synchronization clock across all units.

### 2.4 Acoustic image visualization

A dedicated software application, developed in LabVIEW 2021, is executed on a personal computer to manage the following tasks:

- Coordination and control of the synchronized data acquisition from the 5 sbRIO platforms.
- Storage of the acoustic signals generated by the drone.
- Implementation of beamforming algorithms for the generation of acoustic images.
- Real-time visualization of the resulting acoustic images.

### 2.5 Test set-up

The experimental setup, illustrated in Fig. 3, was deployed outdoors in an open natural environment, free from nearby reflective or noise-generating elements such as trees. The aim was to approximate the acoustic behavior of the drone to that observed in an anechoic chamber. However, several notable differences exist between these conditions. In outdoor settings, environmental factors such as wind introduce disturbances that affect the drone's stability, making it challenging to maintain a fixed position throughout the entire data acquisition process. As a result, each of the six motors compensates independently by adjusting its rotational speed to stabilize the drone. Nevertheless, slight variations in altitude and horizontal (x-y plane) position were observed during the tests.

### 2.6 Data acquisition

Based on the previously described setup, two different experiments—illustrated in Fig. 4—were conducted during the same flight, varying the drone's altitude from approximately 1 to 2 meters above the array. It is important to note that controlling the drone becomes increasingly challenging at higher altitudes due to the previously mentioned environmental disturbances. As a result, the indicated heights are approximate and may vary slightly between captures.

A total of 100 acoustic snapshots were recorded for each height, with a duration of 100 milliseconds per capture, resulting in 10 seconds of data per experiment. To generate the spatial acoustic image, a beamforming algorithm based on the delay-and-sum technique was applied in the frequency domain using the Discrete Fourier Transform (DFT).

**Figure 3**. Test set-up.

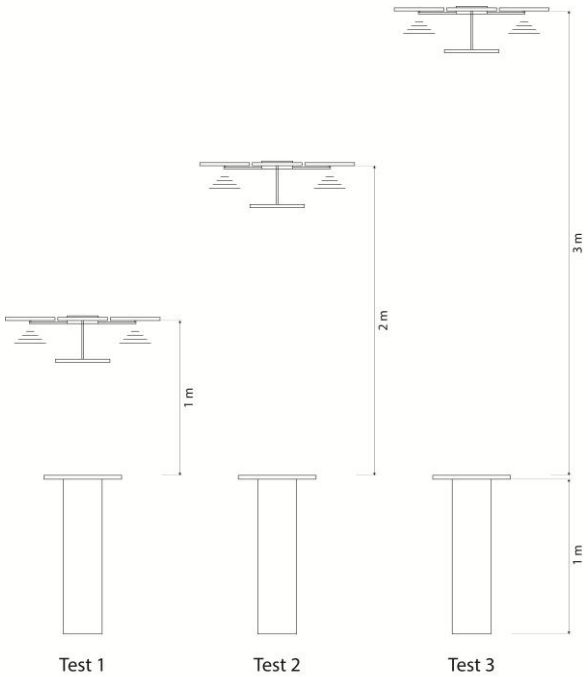


**Figure 4**. Experimental setups of drone hover tests at different altitudes

It should be emphasized that the spatial resolution of the resulting acoustic image primarily depends on four factors: the physical aperture of the array, the inter-sensor spacing, the pointing angle, and the signal frequency. The first two parameters are fixed by the array's geometry and the total number of sensors, and thus cannot be modified. Spatial resolution degrades as the pointing angle increases, which highlights the importance of centering the 2D array with respect to the drone during the measurement process.

## 3. PROCESSING ALGORITHM

The implemented processing algorithm is illustrated in Fig. 5. Initially, the acquired signals are pre-processed, and the beamforming algorithm is applied to generate 4D acoustic images from the recorded data. The focusing distance is defined according to the theoretical height of the drone during the experiment, i.e., either 1 m or 2 m. The analysis is carried out in Cartesian coordinates within the following ranges: x-axis from –0.6 m to 0.6 m, y-axis from –0.6 m to 0.6 m, and frequency from 12 kHz to 48 kHz. In the time domain, the signals are segmented into 2 ms intervals.

Each generated acoustic image, corresponding to a time segment, reflects slight variations in the actual position and height of the drone compared to the theoretical values. These deviations are addressed during the initial processing stage; however, the resulting dataset remains non-uniform, making it necessary to correct both the coordinate system and the focusing distance to ensure spatial consistency across frames.

To solve this problem, a correction parameter is calculated and applied to the beamforming distance. This parameter is obtained by comparing the distance between the drone's propellers in the range and frequency-averaged acoustic image with the known actual value. The beamforming distance is then recalculated for each captured signal, reapplying the beamforming algorithm to obtain a homogeneous group of images where the drone retains its dimensions, regardless of the actual height in the acquisition process. In addition, the position of the geometric center of the drone is calculated so that in all captures the drone is at the origin of coordinates. The corrected 4D images are shown in Fig. 6.

Instead of averaging the acoustic image generated in each 2 ms segment and in each experiment, it was decided to obtain the position of the maxima of each of the blades as a parameter, assuming that each blade is identified with a single maximum of energy. Six circular areas of analysis were established, centered on the position of each propeller.

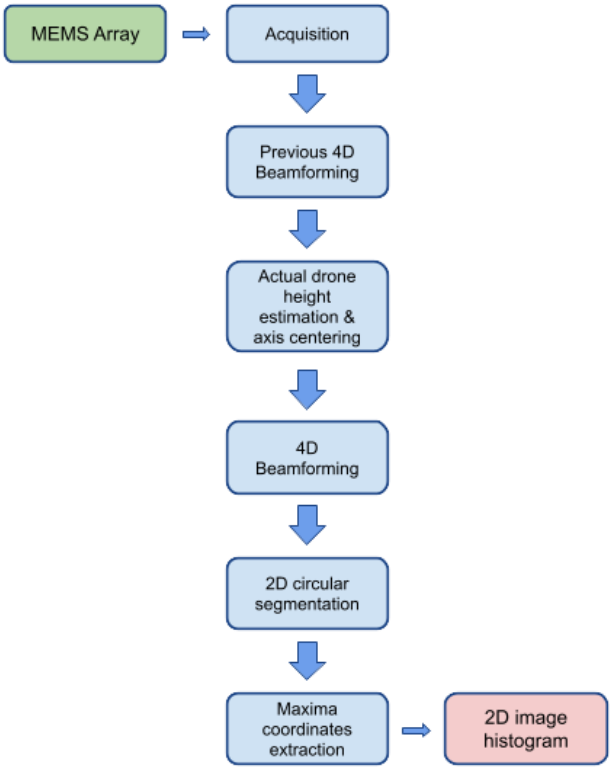


**Figure 5**. Block Diagram of the processing algorithm.

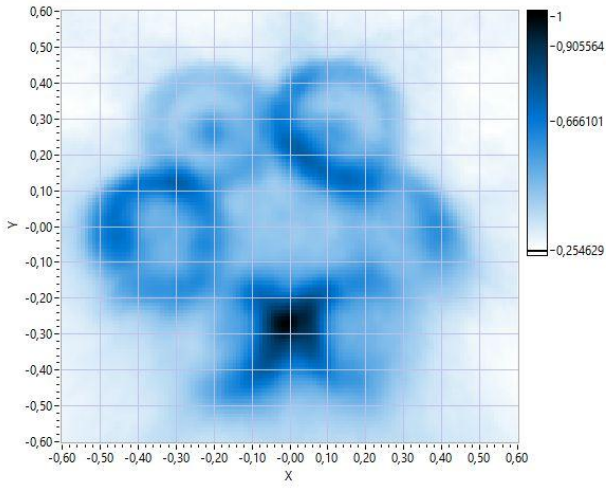


**Figure 6**. Corrected acoustic image.

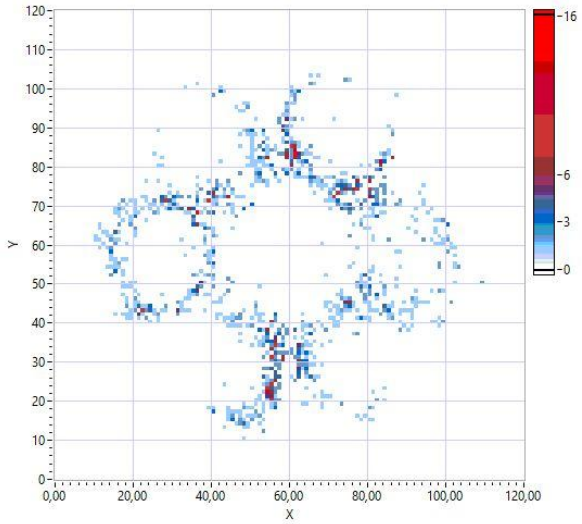


**Figure 7**. Maxima histogram for 20 kHz.

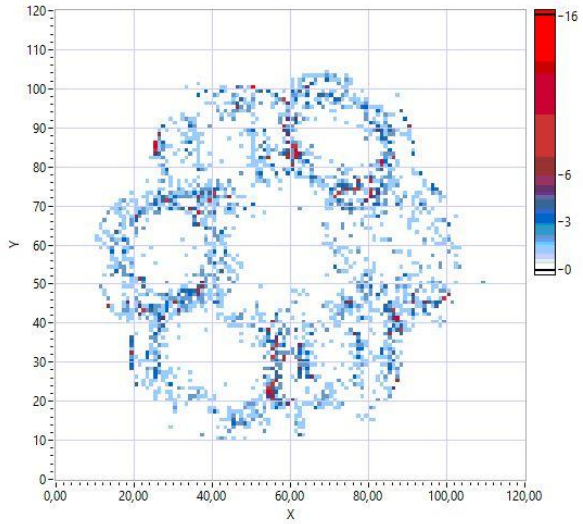


**Figure 8**. Maxima histogram with virtual positions for 20 kHz.

Finally, we assume that if we have an absolute maximum corresponding to the predominant propeller blade, there must be another relative maximum in the opposite blade. Taking the geometric center of each propeller as a reference, we obtain all the maxima generated by the six propellers and their two blades.

## 4. RESULTS

After applying the complete set of algorithms, the identified acoustic peaks were mapped onto a grid of Cartesian coordinates for visualization. To improve visualization and determine the areas where the maxima are concentrated, 2D histograms have been calculated, where the frequency of the maxima is visualized with a color scale (see figures 6 and 7). This technique facilitates a clearer interpretation of the spatial distribution and the density of the maxima throughout the spatial domain of the acoustic images.

## 5. CONCLUSIONS

The results obtained after applying the described algorithm show that the dominant noise contributions originate at the tips of the propellers, as had been proposed in the working hypothesis. In particular, the intersections between adjacent propellers show a significantly higher concentration of acoustic maxima compared to other regions within the plane of rotation.

In addition, a large number of the detected peaks, prior to the aggregation of the peak corresponding to the opposite blade of each propeller, are predominantly found along the inner edge of each propeller. We postulate that this phenomenon is due to interference effects between the propellers and the structural components that support the engines.

These findings open up the possibility of implementing active noise mitigation strategies during sound-based detection missions or emergency operations. Specifically, constrained deterministic beamforming algorithms can be used where it is established that in the positions of the most predominant maxima, nulls are generated in the radiation pattern, enabling a significant reduction in noise generated by the drone itself.

## 6. ACKNOWLEDGMENTS

This research was funded by the Junta de Castilla y León, co-financed by the European Union through the European Regional Development Fund (FEDER) (ref. VA228P20).

## 7. REFERENCES

[1] D. Laurijssen, W. Daems, J. Steckel: "HiRIS: an Airborne Sonar Sensor with a 1024 Channel Microphone Array for In-Air Acoustic Imaging", *IEEE Access*, 2024.

[2] D. T. Berengué, F. Z. Zhou, M. U. Manso, R. G. Pita, M. R. Zurera: "Acoustic localization of UAVs with microphone arrays. Comparison of different array geometries.", *Tecniacústica*, 2023.

[3] G. Sinibaldi, L. Marino: "Experimental analysis on the noise of propellers for small UAV", *Applied Acoustics*, vol. 74, pp. 79-88, 2013.

[4] R. Vijayanandh, M. Ramesh, G. Raj Kumar, U. K. Thianesh, K. Venkatesan, M. Senthil Kumar: "Research of Noise in the Unmanned Aerial Vehicle's Propeller using CFD", *International Journal of Engineering an Advanced Technology*, Vol. 8, Issue 6S, 2019.

[5] K. Oeckel, S. Angermann, A, Frahm, S. Kümmritz, M. Kerscher, G. Heilmann: "Validation of Optoacoustic Propeller Noise Examinations", *Inter Noise*, 2019.

[6] Knowles: "SPH0641LU4H-1 MEMS Microphone". https://www.knowles.com/docs/default-source/model-downloads/sph0641lu4h-1-revb.pdf. Last access: March 18, 2025.

[7] T. He, Q. Pan, Y. Liu, X. Liu, D. Hu: "Near-field beamforming analysis for acoustic emission source localization," *Ultrasonics*, vol. 52, no. 5, pp. 587–92, 2012.

[8] National Instruments: "SbRIO-9607 Platform." https://www.ni.com/docs/en-US/bundle/sbrio-9607-feature/page/overview.html, Last accessed: March 14, 2025.